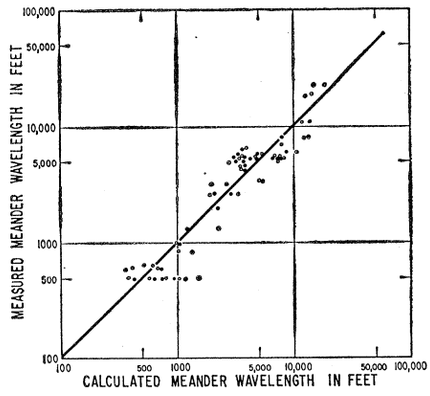

Fig. 3. Relation between measured and calculated meander wavelength from Eq. 1 (data plotted as dots) and Eq. 2 (data plotted as open circles).

ston's data about 98 percent of the variation of the meander wavelength from the mean is explained by mean annual discharge alone, whereas, for the data used here, only 43 percent of the variation of wavelength from the mean is explained by discharge. A possible explanation of this large difference in the coefficient of determination might be that Carlston's data were collected from one type of river, whereas my data were collected from a range of channel types including both bedload and suspended load channels as defined above. The distribution of points on Fig. 1 supports this assumption. The points representative of suspended-load channels, that is, those containing a high percentage of silt and clay (*M*), fall about the regression line, whereas the points representative of bedload channels, those containing a low percentage of silt and clay, plot well above the regression line.

A multiple regression analysis yielded the following equation:

$$l = 1890\, Qm^{0.34}/M^{0.74} \qquad (1)$$

In this equation mean annual discharge (*Qm*) and the percentage of silt-clay in the perimeter of the channels (*M*) explains 89 percent of the variation of wavelength (*l*) from the mean (correlation coefficient = .95; standard error = 0.16 log units), which is a significant improvement over the relation between wavelength and discharge alone and which indicates the influence of the type of sediment load on the meander wavelength.

Meander wavelength is related to the bankfull discharge of many rivers (*8*, *9*) or to a discharge of the order of magnitude of the mean annual flood (*Qma*). Dury's (*9*) regression line relating meander wavelength to bankfull discharge passes through the scatter of points resulting from the plotting of meander wavelength against mean annual flood (Fig. 2). On Fig. 2 the low silt-clay channels plot above his regression line, whereas the high silt-clay channels plot below his regression line.

A multiple regression analysis yields the following equation:

$$l = 234\, Qma^{0.48}/M^{0.74} \qquad (2)$$

In this relation, 86 percent of the variation of meander wavelength from the mean is explained (correlation coefficient = .93; standard error = 0.19 log units), but only 40 percent of the variation is explained by the use of mean annual flood alone.

Significant improvement of the estimation of meander wavelength occurs when a factor representative of type of sediment load is used (Fig. 3), and it is concluded that differences in meander wavelengths between rivers or changes of meander wavelength along a river cannot be attributed to changes of water discharge alone. Instead, a tenfold range in meander wavelength at a given discharge can be attributed to variations in type of sediment load (Figs. 1 and 2).

It has been suggested that the dimensions of meanders are related to channel gradient (*3*, *10*) and width (*8*). However, a simple correlation of stream gradient against meander wavelength is not significant. It is true that the simple correlation of meander wavelength with channel width will be very good, but both are closely related to discharge and type of sediment load (*7*). Therefore, although many river characteristics are interrelated, as are width and meander wavelength, the independent variables that determine both channel width and meander dimensions are discharge and type of sediment load.

S. A. SCHUMM

Department of Geology,
Colorado State University,
Fort Collins 80521

References and Notes

1. S. A. Schumm and R. W. Lichty, *Amer. J. Sci.* **263**, 110 (1965).
2. L. B. Leopold and T. Maddock, Jr., *U.S. Geol. Surv. Prof. Paper* **252** (1953).
3. C. W. Carlston, *Amer. J. Sci.* **263**, 864 (1965).
4. S. Leliavsky, *An Introduction to Fluvial Hydraulics* (Constable, London, 1955), p. 231.
5. S. A. Schumm, *U.S. Geol. Surv. Circular* **477** (1963).
6. E. W. Lane, *Amer. Soc. Civil Eng. Proc.* **81**, paper No. 745 (1955).
7. S. A. Schumm, *U.S. Geol. Surv. Prof. Paper*, in press.
8. L. B. Leopold and M. G. Wolman, *ibid.* **282-B**, 39 (1957).
9. G. H. Dury, *ibid.* **452-C** (1965).
10. J. F. Friedkin, *U.S. Waterways Expt. Sta., Vicksburg* (1945).
11. Publication authorized by the director, U.S. Geological Survey. I thank R. F. Hadley, C. E. Sloan, C. W. Carlston, and C. Nordin, Jr., for their review of the manuscript and R. N. Forbes, Jr., for preparing the illustrations.

20 July 1967

Mercury: Observations of the 3.4-Millimeter Radio Emission

Abstract. *Observations of the 3.4-millimeter radio emission from Mercury during 1965 and 1966 yielded the following relationship between average brightness temperature* T_B *of the disk and the planetocentric phase angle* i:

$$T_B = 277\ (\pm 12) + 97\ (\pm 17)\ \cos [i + 29\ \text{deg}\ (\pm 10\ \text{deg})]\ ^\circ K$$

The errors are statistical standard; the phase shift corresponds to a phase lag —that is, the maximum and minimum of insolation lag the maximum and minimum of planetary radiation.

Observations of Mercury made in 1965 at 3.4 mm (88 Ghz) indicated the absence of any significant difference between the average brightness temperature, T_B, over the disk on the day and night sides (*1*). That is, there was no variation of T_B with phase angle *i*. This unexpected result led us to make much more extensive observations in 1966. The resulting data clearly show a T_B variation with phase angle.

We made observations at 3.4 mm for a total of 410 hours of integration time on 102 days from 5 April through 23 October 1966 with the 15-foot (4.57-m), 2.8-arc-min-beamwidth antenna of the Space Radio Systems Facility of Aerospace Corporation. We used computer-controlled dual-beam observing, data reduction, and calibration procedures identical to those used in 1965 (*1*). As in 1965, no data were taken when Mercury was within 3 arc degrees of the sun. From three to 14 observing cycles, each 26 minutes long, were obtained every day. The daily average antenna temperatures recorded in 1966 ranged from -0.02 ± 0.05 (standard error) °K to $+0.38 \pm 0.04$ °K. Correction factors for atmospheric attenuation ranged from 1.13 to 1.67, the average value being 1.36.

The daily values of T_B for both 1965 and 1966 are shown in Fig. 1. The values represent unequal amounts of integration time. We have not normalized the observed T_B values to Mercury's mean heliocentric distance; if

Mercury were a blackbody, such normalization corrections would amount to $\lesssim 11$ percent. The scatter in the data is large, particularly near superior conjunction ($i = 0$ degrees) when the planetary signal is weakest, but is consistent with the expected scatter due to receiver noise. Despite the scatter, a variation of T_B with i is apparent.

When the five 1965 values before superior conjunction between phase angles 300 degrees and 320 degrees are weighted and averaged they yield a T_B of 144 ± 48 (standard error) °K. This value, to which a high weight was assigned at the time, was the principal datum which influenced the conclusion that the 1965 data showed no significant day-night T_B variation. But two of the five points are negative and are grossly inconsistent with the apparent general phase variation. We extensively scrutinized the data of all 5 days for errors in antenna pointing, ephemeris tracking, data reduction, voltmeter scale factors, calibration, and solar pointing checks, for deleterious antenna sidelobe detection of the sun (which was about 15 degrees away from Mercury at the time), and for spurious negative signals due to time-constant radio sources in the antenna reference beam (by reobserving the positions where Mercury was on the 2 low days). No such errors or effects were found. The distribution of the antenna temperatures of the 54 observing cycles recorded on these 5 days was nongaussian; hence the 144°K value should not have been assigned as high a weight as the formal standard error of 48°K would suggest. Since other points deviate from the mean phase curve as much as these two points, we conclude that it was an unfortunate coincidence that *both* of these low points occurred in the largest set of averaged 1965 data.

All of the T_B values were assigned weights proportional to the amount of integration time and inversely proportional to the atmospheric attenuation correction factor. The values were then grouped into 20-degree intervals of i, and weighted averages were obtained; the results are shown in Fig. 2. The error bars represent formal statistical standard errors computed from the scatter in the antenna temperatures recorded during all of the observing cycles in each 20-degree interval; they are shown to indicate the signal-to-noise ratio.

We assigned to each average T_B a weight inversely proportional to the product of the average atmospheric attenuation correction factor and the square of the statistical standard error. Weighted least-squares fittings of an equation of the form

$$T_B = T_o + \Delta T \cos (i - \phi)\ °\text{K} \qquad (1)$$

where i ranges from 0 degrees (at superior conjunction) to 360 degrees during a synodic period, are (for 1966 data only)

$$T_B = 291\ (\pm 15) + 87\ (\pm 18) \cos [i + 41 \text{ deg } (\pm 13)]\ °\text{K} \qquad (2)$$

and (for 1965 and 1966 data)

$$T_B = 277\ (\pm 12) + 97\ (\pm 17) \cos [i + 29 \text{ deg } (\pm 10)]\ °\text{K} \qquad (3)$$

The statistical standard errors are indicated; the estimated absolute calibration error of the system is 15 percent. The derived negative values of ϕ are consistent with the direct rotation inferred from the radar results (*2*). The solution for the 1965/1966 data is not significantly different than the solution for the 1966 data alone. The dashed error bar point of Fig. 2 was not used in the solution, but using this

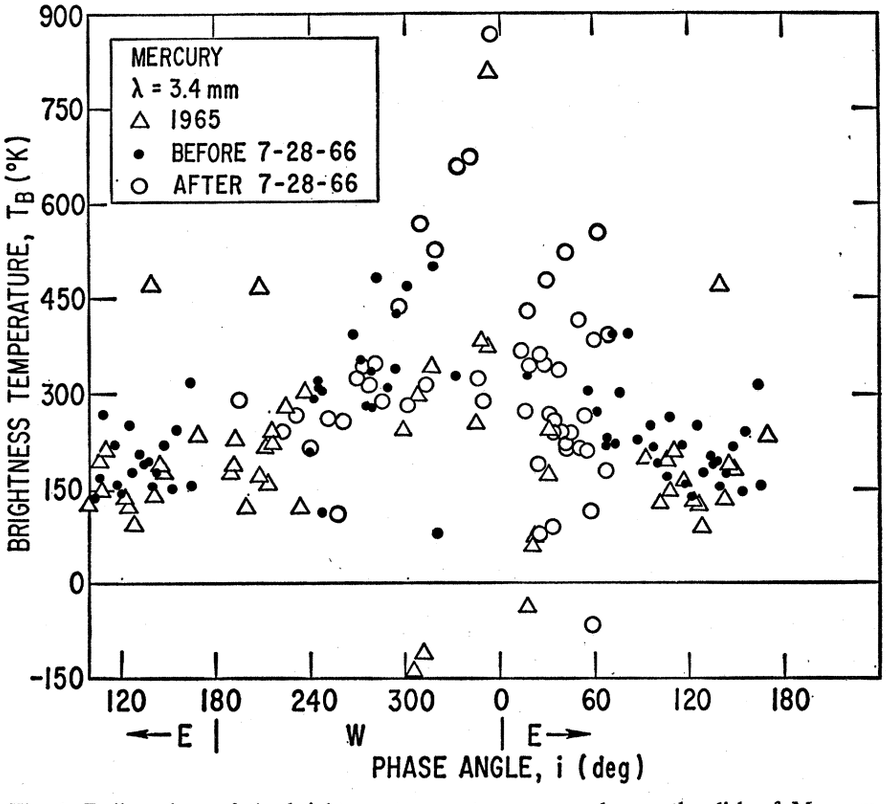

Fig. 1. Daily values of the brightness temperature averaged over the disk of Mercury. The values do not represent equal amounts of integration time. The increased scatter near superior conjunction ($i = 0$ degrees) simply represents the lower signal-to-noise ratios obtained when Mercury is on the opposite side of the sun from the earth. The direction (west or east) toward Mercury relative to the sun is also indicated. The observations represent 200 hours of integration time in 1965 and 410 hours in 1966.

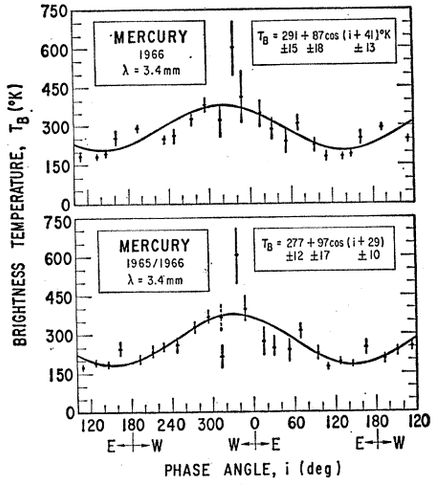

Fig. 2. Daily values of the brightness temperature displayed as weighted averages over 20-degree intervals in phase angle. Averages of the 1966 data alone and the 1965 and 1966 data combined are shown. Error bars represent statistical standard errors. The dashed error bar indicates the average computed by omitting the two negative values of T_B measured before superior conjunction in 1965. The curves shown are the weighted least-squares fits given in the equations. The differences between the fits to the 1966 data and the 1965/1966 data are not statistically significant.

point or omitting some of the lowest weight points, or both, did not yield least-squares solutions significantly different than those of Eqs. 2 and 3.

Mercury's heliocentric distances were not the same during the times of the three superior conjunctions we observed. If Mercury behaved as a blackbody, the differences in the observed T_B values near the three superior conjunctions would have been $\lesssim$ 40°K, a value unfortunately much smaller than the scatter in the data.

Kaftan-Kassim and Kellermann (*3*) have reported 19-mm observations of Mercury made during February and March 1966. Their fit of Eq. 1 yielded

$$T_B = 288\ (\pm\ 17) + 75\ (\pm\ 13)\ \cos [i + 38\ \text{deg}\ (\pm\ 6\ \text{deg})]\ ^\circ\text{K} \quad (4)$$

Using our computing procedure, which differs from theirs, we obtained the following fit to their data:

$$T_B = 294\ (\pm\ 6) + 80\ (\pm\ 8)\ \cos [i + 34\ \text{deg}\ (\pm\ 3\ \text{deg})]\ ^\circ\text{K} \quad (5)$$

The standard errors are indicated.

Both fits to the 19-mm data are in good agreement with the fits to both the 1966 and 1965/1966 3.4-mm data. This good agreement would be puzzling if Mercury behaved at all like the moon. Gary (*4*) has applied to Mercury a horizontally homogeneous, single-layer, thermally independent model that is reasonably consistent with lunar observations. On the basis of the 19-mm Mercury data (which is more precise than the 3.4-mm data) the model predicts a 3.4-mm phase amplitude of 170 ± 15 °K and a phase lag of 16 ± 3 arc degrees; these values are, respectively, much greater than and somewhat less than the observed 3.4-mm values. But Mercury's large orbital eccentricity and the fact that its rotation period is two-thirds of its orbital period suggest that we should not expect Mercury's radio emission to be like that of the moon. A more complex model will be necessary to predict how dissimilar the two Mercury phase curves should be.

E. E. Epstein
S. L. Soter*
J. P. Oliver†
Aerospace Corporation, El Segundo, California
R. A. Schorn
Jet Propulsion Laboratory, Pasadena, California
W. J. Wilson
Space Systems Division, U.S. Air Force, Los Angeles Air Force Station, Los Angeles, California

References and Notes

1. E. E. Epstein, *Science* **151,** 445 (1966).
2. G. H. Pettengill and R. B. Dyce, *Nature* **206,** 1240 (1965).
3. M. A. Kaftan-Kassim and K. I. Kellermann, *Nature* **213,** 272 (1967).
4. B. Gary, in preparation.
5. This work was supported by the U.S. Air Force under contract No. AF 04(695)-1001. R.A.S. was supported in part by the Jet Propulsion Laboratory, California Institute of Technology, Pasadena, under NASA contract No. NAS 7-100. Only through the efforts of G. G. Berry, T. T. Mori, and W. A. Johnson in maintaining and improving the Space Radio Systems Facility equipment has it been possible to carry out the extensive observations necessary to obtain these results.
* Present address: Center for Radio Physics and Space Research, Cornell University, Ithaca, New York.
† Also at the University of California, Los Angeles.
5 July 1967

Knoll and Sediment Drift near Hudson Canyon

Abstract. *A parallel-bedded accumulation of sediments forms a low ridge on the upcurrent side of a partially moated knoll. These sediments were deposited beneath a southwestward-flowing current where it is locally decelerated by the obstructing knoll.*

A newly discovered knoll (*1*) protruding 1000 m above the continental rise off the eastern United States represents the top of a huge peak that has been gradually buried by several kilometers of sediments (Fig. 1) (*2*). A ridge, 30 km long, 5 km wide, and 40 meters high, lying parallel to the regional isobaths, trends northeastward from the knoll to the natural levee of Hudson

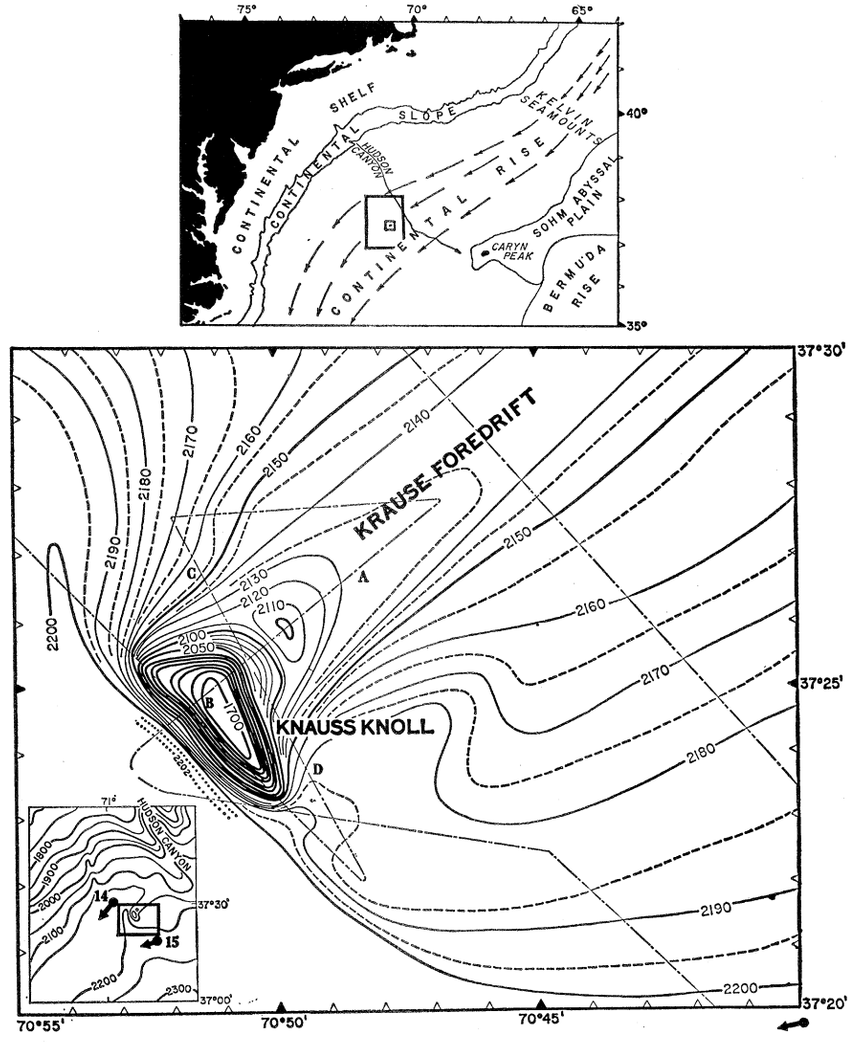

Fig. 1. A knoll on the continental rise of the eastern United States; contours in standard echo-sounding units of 1:400 seconds travel time. Numbers *14* and *15* (inset) refer to bottom photographs; arrows indicate direction of current inferred from scour marks. Profiles illustrated in Fig. 2 are indicated by *A, B, C,* and *D*.